applied sciences

MDPI

Article

Facile Synthesis of Copper Oxide-Cobalt Oxide/Nitrogen-Doped Carbon (Cu_2O-Co_3O_4/CN) Composite for Efficient Water Splitting

Zaffar Ahmed Shaikh [1,*], Nikita Moiseev [2], Alexey Mikhaylov [3] and Serhat Yüksel [4]

1 Faculty of Computing Sciences & Information Technology, Benazir Bhutto Shaheed University, Lyari, Karachi 75660, Pakistan
2 Department of Mathematical Methods in Economics, Plekhanov Russia University of Economics, 117997 Moscow, Russia; mr.nikitamoiseev@gmail.com
3 Financial Research Institute of Ministry of Finance of the Russian Federation, 127006 Moscow, Russia; alexeyfa@ya.ru
4 The School of Business, Istanbul Medipol University, 34810 Istanbul, Turkey; serhatyuksel@medipol.edu.tr
* Correspondence: zashaikh@bbsul.edu.pk; Tel.: +92-333-711-3817

Abstract: Herein, we report a copper oxide-cobalt oxide/nitrogen-doped carbon hybrid (Cu_2O-Co_3O_4/CN) composite for electrochemical water splitting. Cu_2O-Co_3O_4/CN is synthesized by an easy two-step reaction of melamine with Cu_2O-Co_3O_4/CN composite. The designed composite is aimed to solve energy challenges by producing hydrogen and oxygen via electrochemical catalysis. The proposed composite offers some unique advantages in water splitting. Carbon imparts superior conductivity, while the water oxidation abilities of Cu_2O and Co_3O_4 are considered to constitute a catalyst. The synthesized composite (Cu_2O-Co_3O_4/CN) is characterized by SEM, EDS, FTIR, TEM, and AFM in terms of the size, morphology, shape, and elemental composition of the catalyst. The designed catalyst's electrochemical performance is evaluated via linear sweep voltammetry (LSV) and cyclic voltammetry (CV). The Cu_2O-Co_3O_4/CN composite shows significant electrocatalytic activity, which is further improved by introducing nitrogen doped carbon (current density 10 mA cm^{-2}, onset potential 91 mV, and overpotential 396 mV).

Keywords: water splitting; hydrogen evolution reaction; oxygen evolution reaction; electrocatalyst; Cu_2O-Co_3O_4/CN composite

Citation: Shaikh, Z.A.; Moiseev, N.; Mikhaylov, A.; Yüksel, S. Facile Synthesis of Copper Oxide-Cobalt Oxide/Nitrogen-Doped Carbon (Cu_2O-Co_3O_4/CN) Composite for Efficient Water Splitting. *Appl. Sci.* **2021**, *11*, 9974. https://doi.org/10.3390/app11219974

Academic Editors: María Linares and María Orfila

Received: 8 September 2021
Accepted: 22 October 2021
Published: 25 October 2021

1. Introduction

The world is facing an energy crises nowadays. A rough estimation shows that, in 2050, the energy consumption will be doubled when compared to 2020 [1]. Now, the world is dependent on nonrenewable energy sources to meet energy requirements [2]. However, with the increase in energy prices, energy demand, and global warming, researchers are thinking about renewable energy resources [3,4]. The main reasons for the increase in energy demand are the world's high growth rate and a great industrial revolution. Throughout the whole history of humankind, humans used energy from fossil fuels. In the past, only two types of fossils (wood and charcoal) were used, but, due to the industrial revolution, many more options, including oil, coal, and natural gas [5,6], have also been used to meet the energy requirements. According to a survey, fossil fuel reservoirs have been enough for decades, but, with time, these reservoirs are depleting [7,8].

Modern day research is focused on developing renewable energy sources, and water splitting is a promising source of energy [9,10]. There has been a noticeable increase in oxygen evolution reaction (OER) in recent years, and it is estimated that this increase will be doubled in future years [11,12]. The conventional method of hydrogen and oxygen output involves a steam reforming method [13]. Nowadays, O_2 is also produced by using the photocatalytic method. In these methods, sunlight is used to create oxygen and hydrogen

molecules. Solar water splitting methods of oxygen and hydrogen production include thermochemical and photobiological methods [14,15].

In the water-splitting process, sunlight is used as an energy source, and a water molecule is used as an electron donor to complete fuel cells [16]. Two half reactions are involved: the first one is the hydrogen evolution reaction, and the second one is the oxygen evolution reaction. Different types of charge separators are used to enhance the rate of reaction. Some of the charge separators are semiconductors, such as nanobelts, nanotubes, nanowires, and nanosheets [17,18]. Hetrojunction semiconductors are also being used for better charge separation. Cobalt is commonly used as a catalyst in hydrogen and oxygen evolution reactions [19]. Photolytic corrosion is the main problem in these reactions. This problem can be minimized by increasing electrodes' stability and providing more active sites for the photocatalytic activity of hydrogen and oxygen [20]. Researchers are exploring other options, such as nitrides, phosphides, selenides, and carbides [21,22]. These types of non-nobel metal catalysts show high corrosion resistance and better electroconductivity [23–28]. Some highly efficient catalysts recently reported for HER are CoS_2, FeS_2, $MoSe_2$, g-C_3N_4/Co-MOF (ZIF-67), g-C_3N_4/Nb_2O_5**,** CdS QD/MoO_3–OV/g–C_3N_4, and NiS_2 [1–4].

Nanotubes and nanosheets are used to increase active sites for electrocatalytic HER nanowires [28,29]. Metal carbides show similar behavior, in terms of catalytic properties and electronic band. Due to these reasons, carbides show high hydrogen adsorption and maximum electrical conductivity [30]. Due to the presence of a d-band structure, they show high electrical conductivity and low hydrogen adsorption capacity. Mo_2C and WC are both categorized as non-Pt catalysts for hydrogen evolution reactions. These have been tested at different pH ranges and proved to be a stable support for HER [31].

Some catalysts can perform both oxygen and hydrogen evolution reactions [32,33]. Pt, Rh, and Ir-based catalysts can serve as bifunctional catalysts, but such types of catalysts are lower in number and have very high costs [34]. The great challenge in this field is to find a low cost, easily available bifunctional catalyst that can work both in acidic and basic environments [35,36]. The last few years' foci have been shifted to a low cost and earth abundant transition metal, transition metal oxide, transition metal sulfides, transition metal nitrides, and transition metal carbides [37]. The most common metals used in these catalysts are iron, nickel, copper, and cobalt [38]. The catalysts prepared by these metals' combinations have an exceptional ability for electrochemical water splitting and show improved reaction kinetics, fast charge transfer, and high conductivity. Cobalt based catalysts have been frequently used in water splitting and electrocatalysis [39–41]. The catalysts' conductivity can be further enhanced by adding some dopants, such as nitrogen [42]. Melamine is a well known and common precursor for the preparation of nitrogen-doped carbon [43–45].

This study aims to synthesize an effective electrocatalyst for the oxygen evolution reaction (OER). Copper oxide-cobalt oxide/nitrogen-doped carbon hybrid (Cu_2O-Co_3O_4/CN) composite is synthesized by a simple two-step method using low cost precursors. The material is characterized by different analytical techniques and applied for electrochemical water splitting.

2. Experimental

2.1. Chemical and Reagent

Cobalt chloride hexahydrate ($CoCl_2 \cdot 6H_2O$), trisodium citrate ($Na_3C_6H_5O_7$) 99%, Nafion solution ($C_7HF_{13}O_5S$) 5%, glycine ($C_2H_5NO_2$) 99.9%, potassium dihydrogen phosphate (KH_2PO_4) 99%, ethanolamine (C_2H_7NO) 98%, copper sulphate pentahydrate ($CuSO_4 \cdot 5H_2O$) 99%, potassium hydroxide (KOH) 99%, dipotassium hydrogen phosphate (K_2HPO_4) 99%, and hydrogen peroxide 30% (H_2O_2) were purchased by Sigma Aldrich. Ethylene glycol ($C_2H_6O_2$) 99.0% was obtained from Merck. Sulfuric acid (H_2SO_4) 98% was purchased from Riedel-de Haën.

2.2. Synthesis of Cu_2O-Co_3O_4/CN Composite

In the first step, the Cu_2O-Co_3O_4 composite was synthesized by using a reported method [46]. Briefly, a 0.5 mM solution of $CuSO_4 \cdot 5H_2O$ was prepared in 20 mL of water. A quantity of 13 mL of ethanol was added and stirred vigorously to form a clear solution. Then, 1 mM solution of $CoCl_2 \cdot 6H_2O$, 10 g of trisodium citrate, 3 mL of 200 mL solution of KOH, and 0.3 mM solution of glycine were added to the reaction mixture. After vigorous stirring for a half hour, the reaction mixture was transferred to a Teflon lined stainless-steel autoclave. The autoclave was placed in a temperature programmed electric oven, and the mixture was kept for 12 h at 180 °C. After cooling to room temperature, the obtained product was filtered and washed several times with deionized water to remove the unreacted chemicals. The product was dried at 50 °C for 6 h in a vacuum oven. The dried product was calcined at 300 °C for 2 h to obtain Cu_2O-Co_3O_4 composite.

For the synthesis of Cu_2O-Co_3O_4/CN composite, 40 g of melamine, 1 g of glucosamine hydrochloride were mixed with Cu_2O-Co_3O_4 composite, and 400 mL water was added. The mixture was heated at 80 °C till the water was dried. The solid product was ground and heat treated at 400 °C and 500 °C under a nitrogen atmosphere. The obtained product was cooled to room temperature and stored for further use.

2.3. Characterization of Composite

SEM analysis was carried out on a Hitachi SEM S-4700, Japan. For the TEM imaging, the Jeol JEM-F200 Multi-purpose Electron Microscope was used, equipped with an EDS detector. AFM images were recorded on a Bruker AFM (MultiMode 8-HR), Bruker, Germany. FTIR spectrum was recorded in transmission mode on Nicolet iS10 ThermoScientific, Germany.

2.4. Electrochemical Water Splitting

The electrochemical experiments were carried out on two modes of electrochemical workstations; cyclic voltammetry (CV) and linear swap voltammetry (LSV). CV measurements were performed on a three electrode system, standard electrode (Pt wire), reference electrode (Ag/AgCl), and the working electrode. Cu_2O-Co_3O_4/CN composite was deposited on a glassy carbon electrode (working electrode) with a diameter of 3 mm. The synthesized catalyst's electrochemical activity was studied in alkaline media (1 M KOH solution). Different electrochemical parameters, including potential window, scan rate, and pH, were also optimized to achieve maximum efficiency. The selected window range was from −1.0V to +1.0V, and the scan rate was 0.06 mV/s to 0.1 mV/s. The slurry for the glassy carbon electrode was prepared by mixing 4 mg of synthesized catalyst, 80 µL of Nafion, which acts as a binder, and 1 mL of water. This mixture was sonicated to form a dispersion for 30 min. This dispersion was then loaded onto the working electrode and dried at room temperature.

3. Results and Discussion

3.1. Characterization of Cu_2O-Co_3O_4/CN Composite

The synthesized Cu_2O-Co_3O_4/CN composite was characterized by transmission electron microscopy (TEM), scanning electron microscopy (SEM), atomic force microscopy (AFM), energy dispersive X-ray spectroscopy (EDS), and Fourier transform infrared spectroscopy (FTIR). The morphology and particle size of the Cu_2O-Co_3O_4 and Cu_2O-Co_3O_4/CN composites were first characterized by TEM. TEM images of the Cu_2O-Co_3O_4 and Cu_2O-Co_3O_4/CN composites are shown in Figure 1a,b, respectively. From both the images, it is evident that each composites' morphology is different from the other. This is due to an additional layer of nitrogen doped carbon on the Cu_2O-Co_3O_4 composite. The calculated particle size is in the range of 80–100 nm. The morphology was also justified by SEM (Figure 1c,d) and AFM (Figure 1e,f). In the Cu_2O-Co_3O_4 composites, particles are visible, and they are semispherical. However, after the addition of CN, there is a clear change in shape and morphology. This is formed by calcination at higher temperatures. AFM results show the surface of the products: the Cu_2O-Co_3O_4 is rough as compared

to the Cu_2O-Co_3O_4/CN composite, which has a slightly smoother surface with fewer grooves. The elemental composition of the materials was determined by EDS analysis, which indicates the mass percentage of copper (41%), cobalt (33%), and oxygen (21%) in the Cu_2O-Co_3O_4 composite. On the other hand, carbon (24%), nitrogen (11%), oxygen (17%), copper (27%), and cobalt (21%) are present in the Cu_2O-Co_3O_4/CN composite.

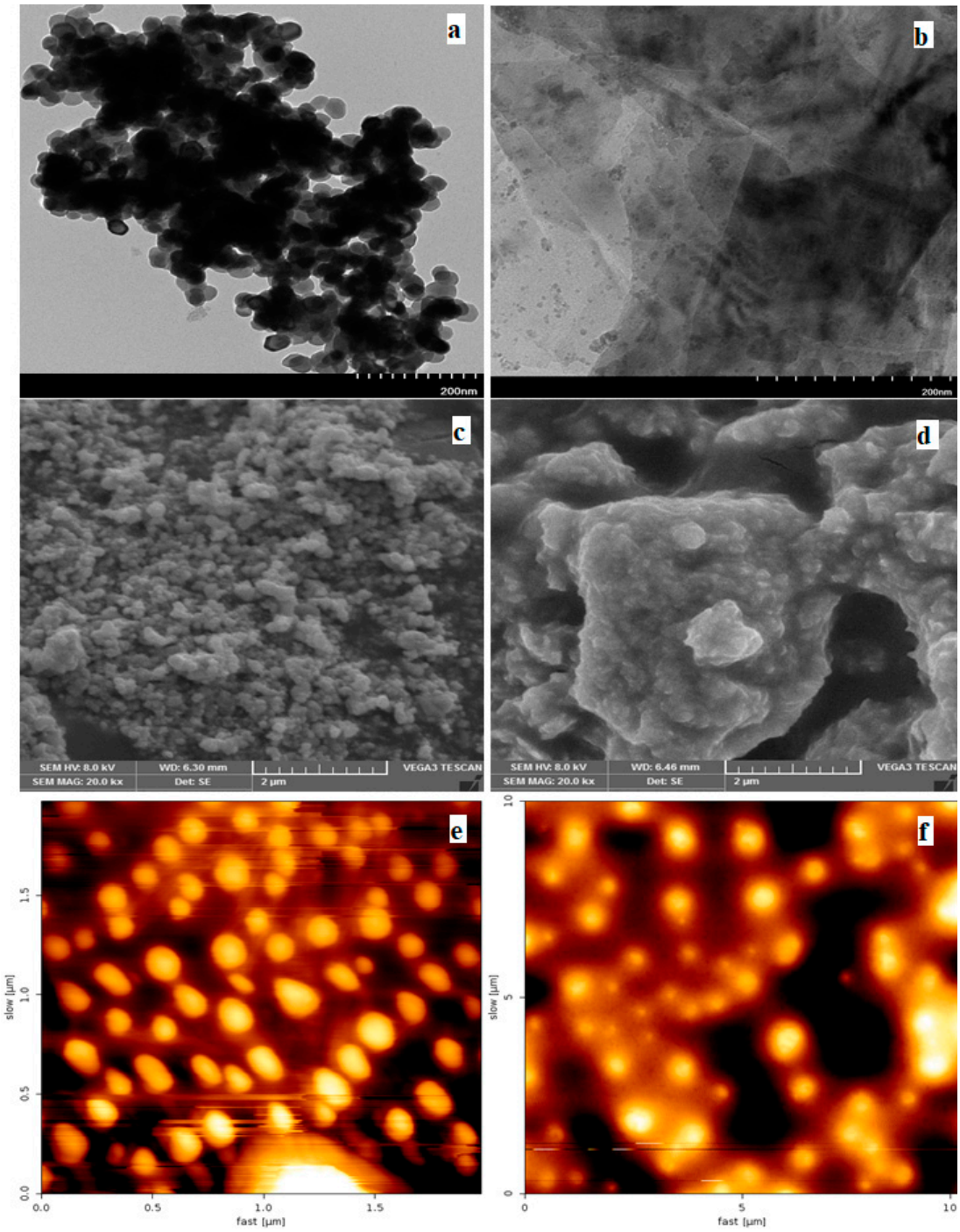

Figure 1. TEM, SEM, and AFM images of Cu_2O-Co_3O_4 (**a**,**c**,**e**) and Cu_2O-Co_3O_4/CN composites (**b**,**d**,**f**).

FTIR analysis was carried out in transmittance mode to confirm the formation of composites (Figure 2). The transmittance peaks at 645 cm^{-1} and 540 cm^{-1} belongs to cobalt oxide and copper oxide, and it is present in both materials, while the peak at 1100 cm^{-1} is due to the presence of -O-C-O- vibrations [41]. The peak presence at 3300 cm^{-1} is due

to hydroxyl groups, which are abundantly present on the surface of metal oxides. The FTIR results confirm the C=O bond of amide as the peaks appearing at 1668 cm^{-1} and 1570 cm^{-1}, which indicates the stretching and bending of C=O. The peak at 1418 cm^{-1} indicates the presence of a hydroxyl group, and the symmetrical vibration peaks at 1635.74 cm^{-1} and 1733.65 cm^{-1} belong to C=O and C=N bands, respectively. The peak at 1703 cm^{-1} shows the interaction between the carbonyl group and the metal ions. The peaks for the metals' coordination with COO appear at 1560 cm^{-1} and 1560 cm^{-1}, respectively.

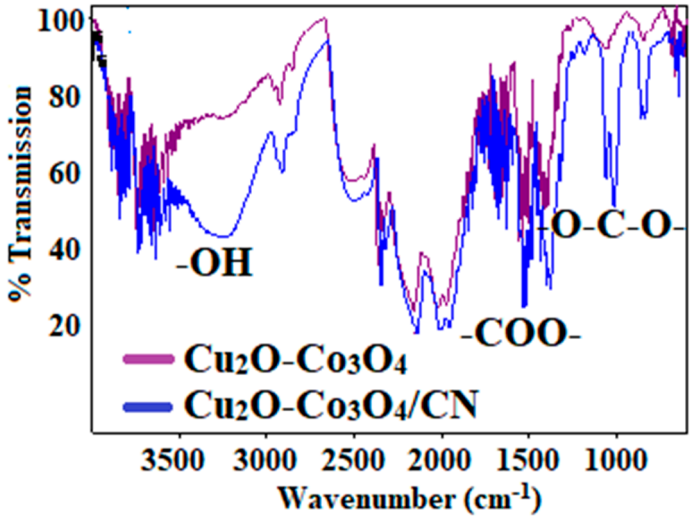

Figure 2. FTIR of Cu_2O-Co_3O_4 and Cu_2O-Co_3O_4/CN composites.

3.2. Electrochemical Water Splitting by Cu_2O-Co_3O_4/CN Composite

The electrochemical activity of the Cu_2O-Co_3O_4/CN composite on a glassy carbon electrode was studied using linear sweep and cyclic voltammetry for water splitting. To obtain maximum efficiency, different parameters, such as scanning rate, potential window, and pH, were optimized for both Cu_2O-Co_3O_4 and Cu_2O-Co_3O_4/CN composites. Initially, the pH of the electrolyte solution was optimized. The blank solution's electrochemical response and all the synthesized materials, including Cu_2O-Co_3O_4, CN, Cu_2O-Co_3O_4/CN at 400 °C, and 500 °C, were recorded at different pHs (7, 7.4, and 8). The figure shows that the composite shows maximum redox potential at pH 8. The electrochemical response of these catalysts is low, at 7 and 7.4. These results show that the current density of the synthesized composite at optimized conditions increases in the scan rate, from 0.06 mV/s to 0.1 mV/s.

The catalyst was prepared in a slurry and applied to GCE via micropipette. Then, the effect of catalyst volume was evaluated. Figure 3 explains the linear calibration curve and the volumetric activity of the synthesized catalyst. Different concentrations of Cu_2O-Co_3O_4/CN give reversible cyclic voltammetric peaks, showing reduction as well as oxidation peaks. With the increasing volume of the catalyst, from 0.1 µL to 0.5 µL, the oxidation peak current (Ipa) increases from 2.99 µA to 5.879 µA. Cu_2O-Co_3O_4/CN shows a peak potential (Epa) of 0.138 V, in comparison to 0.608 V for blank. Peak currents for different volumes of the catalyst, from 0.1 µL to 0.5 µL, are −4.104 µA, −4.505 µA, −5.764 µA, −7.514 µA, and -9.605 µA, respectively. For the Cu_2O-Co_3O_4/CN composite, the cathodic peaks potential (EPC) is −0.018 V. Reduction and oxidation rates increase as the amount (volume of slurry) of synthesized catalyst increases. The reason is that, as the composite amount increases, the active sites for reduction and oxidation reaction also increase. The relationship between current and concentration is linear at pH 8, as shown in Figure 3b. R^2 obtained for reduction and oxidation are 0.959 and 0.91, respectively.

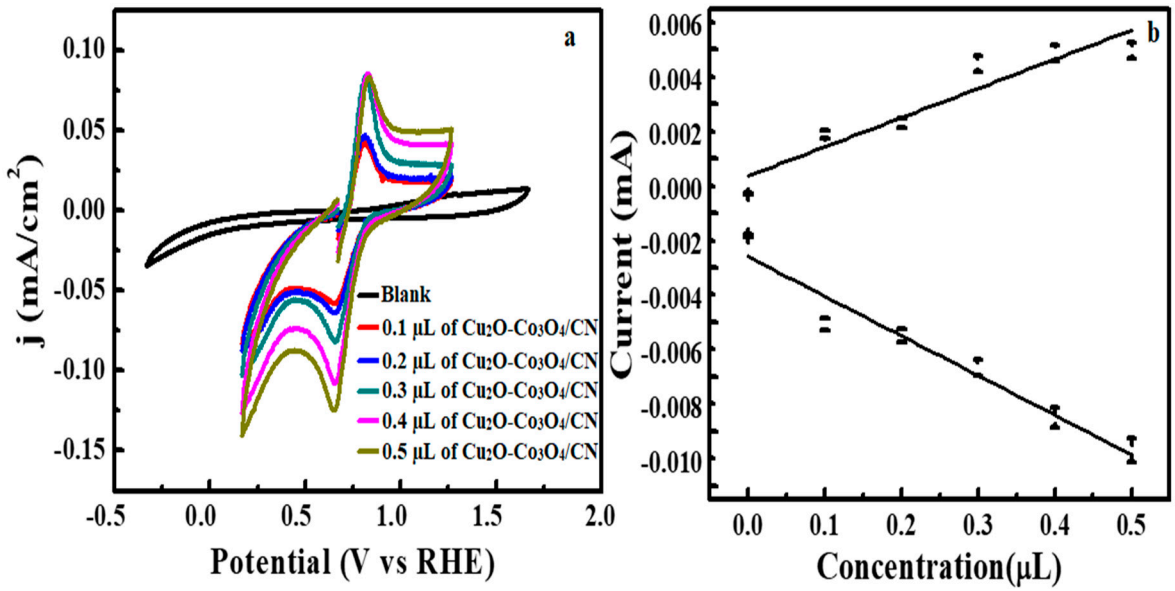

Figure 3. (**a**) CV curves of Cu_2O-Co_3O_4/CN composite at slurry volume range from 0.1 to 0.5 µL in 1 M KOH; (**b**) linear calibration curve for oxidation and reduction at different concentrations.

The electrochemical activity of nitrogen doped carbon was monitored at different scan rates in 1 M KOH. Different ranges of current were obtained at different scan rates (Figure 4a). Initially, a 0.06 mV/s scan rate was set for electrochemical analysis and the redox phenomenon was observed in the voltammogram (0.618 V for oxidation and −1.101 V for reduction). The current obtained due to oxidation is 0.0458 mA, and for reduction is −0.0334 mA. The potential difference (ΔE) is −1.710 V. This scan rate is very slow and consumes more time. The deposition and the results are not accurate, due to surface damage. The peak current for both oxidation and reduction increased at higher scan rates, as shown in Figure 5b. R^2 for oxidation and reduction are 0.891 and 0.846, respectively. These results indicate that electrochemical activity is directly proportional to the scan rate.

The linear sweep voltammetry response in 1M KOH was also evaluated (Figure 4c), and a similar trend was obtained. The obtained current density is 0.890 mA/cm^2, and the Tafel slope is 334 mV/decade (Figure 4d). Moreover, at η (overpotential) = 0.58876 V, current density is 1 mA/cm^2. The reversible potential of OER is 1.19 and 0 V vs. reference electrodes, respectively. Therefore, as current density increases, the electrocatalytic activity of the material rises with the scan rate.

Similarly, the electrochemical response of Cu_2O-Co_3O_4 composite was also measured in 1M KOH solution, using CV and LSV (Figure 6). A mild redox phenomenon is detected at a scan rate of 0.06 mV/s (Figure 5a). As the scan rate rises, the corresponding reduction and oxidation peaks are detected. The highest peak current is observed at 0.1 mV/s (Epa = −0.0884 V with Ipa = 3.21 mA and Epc = −0.9676 V at Ipc = −2.13 mA). The calibration curve for the scan rate vs. the corresponding current is presented in Figure 6b. The obtained curve for oxidation has a slope of 0.06355 with a standard error of 0.00562 and R^2 = 0.96744. The correlation coefficient for reduction is 0.8742. LSV curves for the Cu_2O-Co_3O_4 composite at different scan rates are shown in Figure 6c. At 0.1 mV/s, it shows the start potential of 1.64 V in OER's direction, and has an anodic current that increases quickly when the extra potential is given. The experiment's outcome indicates that the possible start of the Cu_2O-Co_3O_4 composite is near the OER's thermodynamic potential. Therefore, the Cu_2O-Co_3O_4 composite provides a Tafel slope and a current density of 3.89 mA/cm^2. Moreover, the η (overpotential) obtained from the Cu_2O-Co_3O_4 composite is 0.370 V, with a current density of 1.07 mA/cm^2 (Figure 5d).

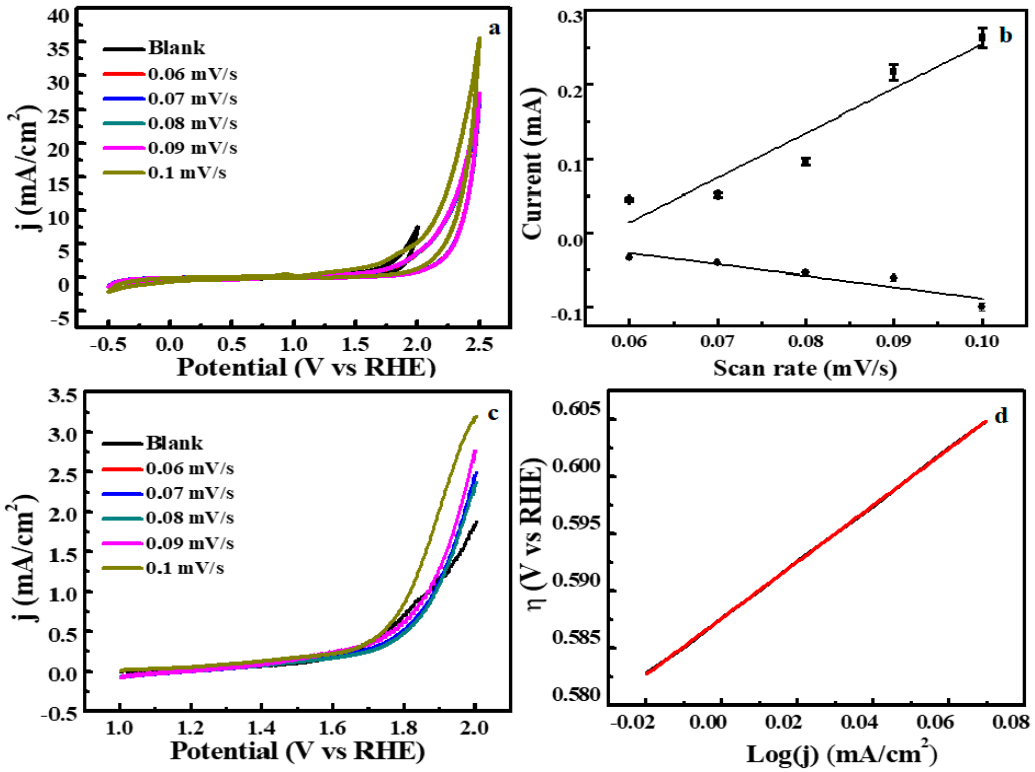

Figure 4. (**a**) Cyclic voltammogram and (**b**) calibration curve; (**c**) LSV curves and (**d**) the corresponding Tafel plots of nitrogen doped carbon at different scan rates in 1 M KOH.

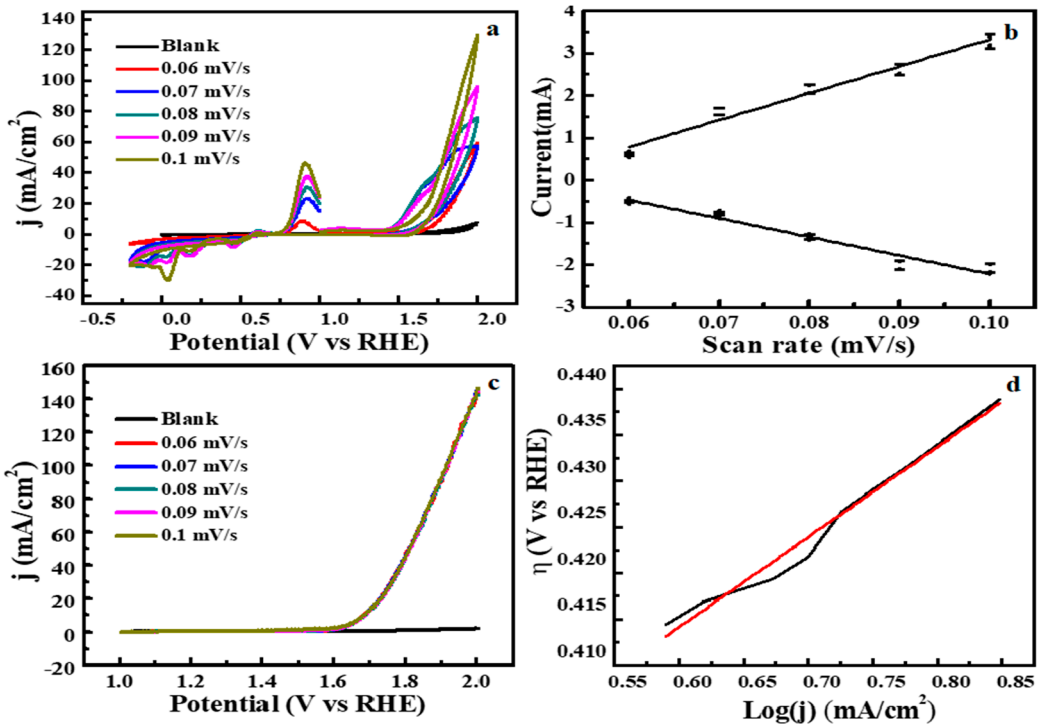

Figure 5. (**a**) LSV curves for Cu_2O-Co_3O_4 composite and the (**b**) calibration curve, (**c**) LSV curves, and (**d**) the corresponding Tafel plots for Cu_2O-Co_3O_4 composite, in 1 M KOH, at different scan rates.

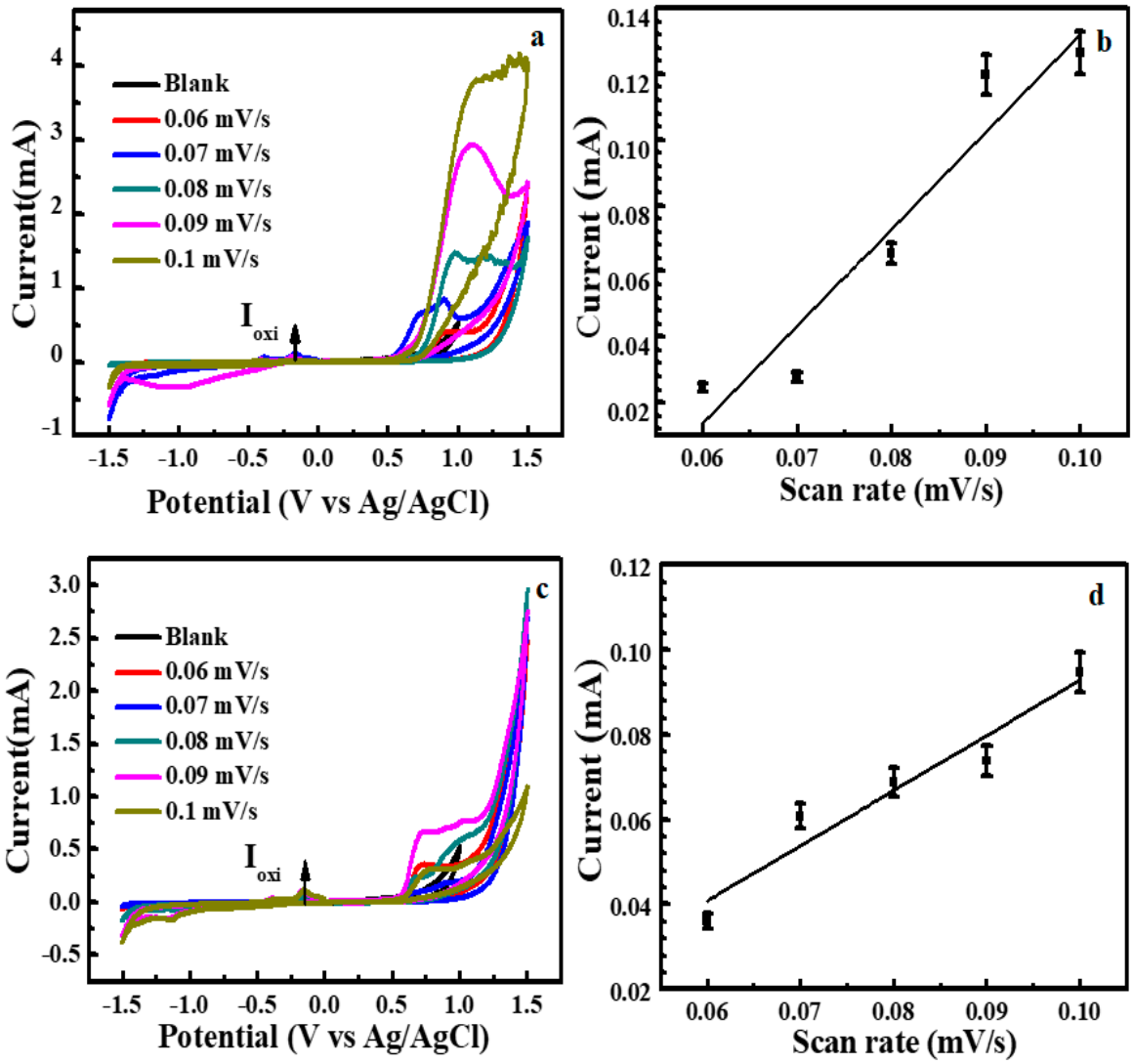

Figure 6. Effect of scan rate on electrochemical performance of Cu_2O-Co_3O_4/CN composite synthesized (**a**) at 400 °C, (**b**) its calibration curve; (**c**) at 500 °C, and (**d**) its calibration curve obtained at scan rates in 1 M KOH.

The effect of the scan rate electrochemical activity of the Cu_2O-Co_3O_4/CN composite synthesized at 400 °C and 500 °C was also studied in 1 M KOH. The voltammograms obtained for the Cu_2O-Co_3O_4/CN composite synthesized at different temperatures are different from each other, which indicates that the temperature played a significant role in the formation of the final product. Figure 6a,c present the effect of the scan rate on the cyclic voltammograms of the Cu_2O-Co_3O_4/CN composite synthesized at 400 °C and 500 °C. As discussed previously, at lower scan rates, a lower amount of current is produced, which increased with increasing scan rates and, finally, reached a maximum point at a scan rate of 0.1 mV/s. Calibration curves are plotted between scan rates, and currents are shown in Figure 6b,d for the Cu_2O-Co_3O_4/CN composites synthesized at 400 °C and 500 °C, respectively. The obtained correlation coefficients are 0.7924 and 0.96502, respectively.

LSV experiments on the Cu_2O-Co_3O_4/CN composite electrodes were studied in the 1M KOH solution. The effect of different scan rates on the LSV response of the Cu_2O-Co_3O_4/CN composite synthesized at different temperatures is shown in Figure 7. Although the pattern is the same, the current density and Tafel slopes of the nitrogen doped carbon and the Cu_2O-Co_3O_4/CN composite are different. A current of 0.1 mV/s shows a start potential of 1.682 V toward OER; the anodic current shows a rapid increase as the potential is applied. The catalyst synthesized at 400 °C shows better efficiency, as compared to the product synthesized at 500 °C. The main reason for the better efficiency of Cu_2O-Co_3O_4/CN

composite at 400 °C could be better electron transfer due to the higher conductivity of metal oxides and nitrogen doped carbon, and a higher surface area. The Tafel slope for the product synthesized at 400 °C is 281 mV/decade and the current density is 0.599 mA/cm^2, as shown in Figure 7b. In addition, a current density of 10 mA/cm^2 was recorded at η (overpotential) = 396 mV. These experiments explain the good electrocatalytic response of the Cu_2O-Co_3O_4/CN composite toward OER. Similarly, at 500 °C, the overall catalytic performance is low. OER's onset potential is 1.6194, Tafel slope 261 mV/decade and current density 0.771 mA/cm^2, as shown in Figure 7c,d.

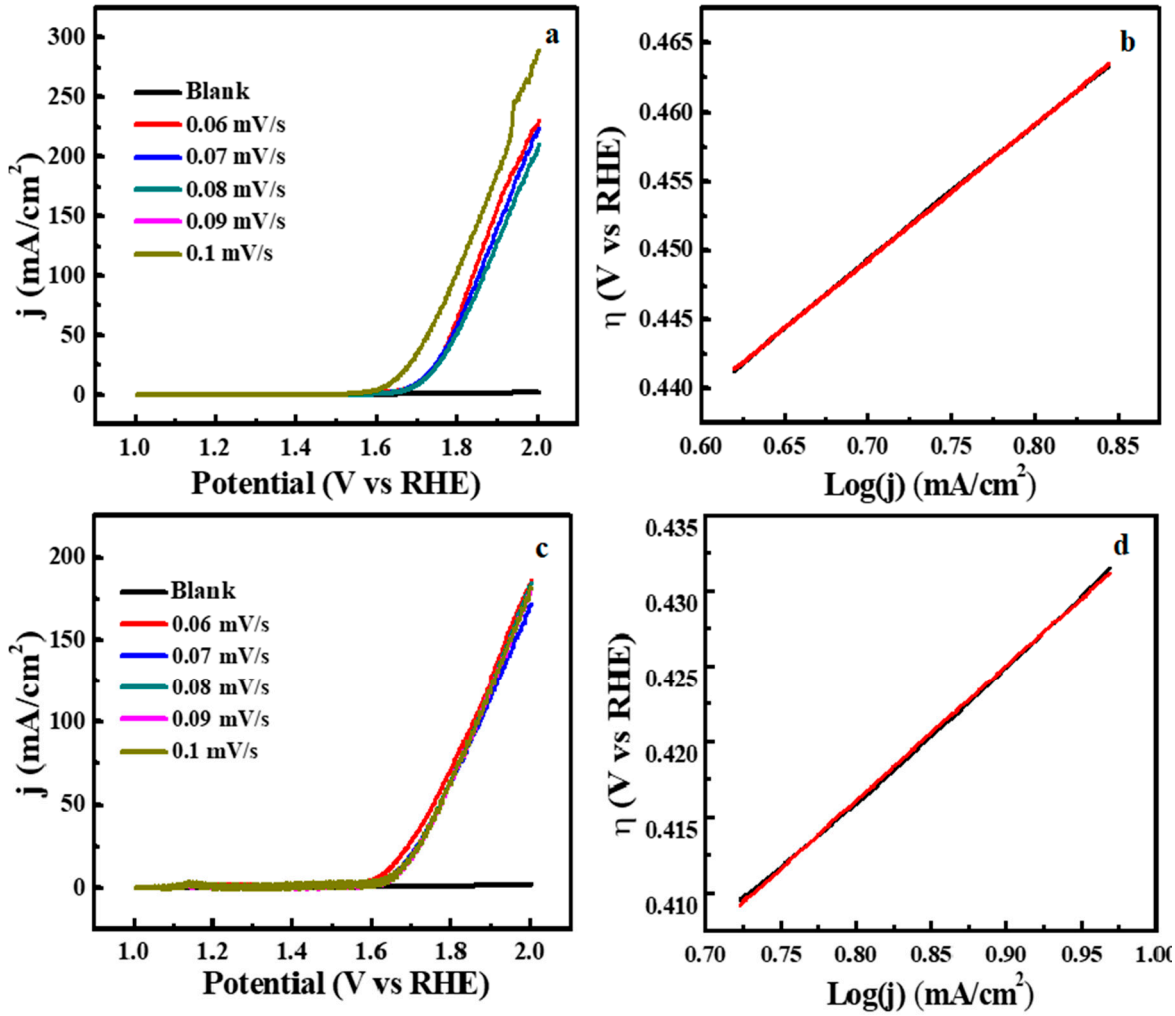

Figure 7. LSV curves of Cu_2O-Co_3O_4/CN composite synthesized at (**a**) 400 °C and (**c**) 500 °C and corresponding Tafel slops (**b**,**d**) at different scan rates, in 1 M KOH.

Using Ag/AgCl as the reference electrode for electrolytes is commonplace in potentiometry and voltammetry, and their importance in the chemical laboratory is unquestionable. Ag/AgCl electrodes are usually more effective for many purposes.

The electrochemical performance of Cu_2O and Co_3O_4 particles and their different composites is well documented in literature [47–53]. Similarly, the electrical conductivity of nitrogen doped carbon is also reported [54–58]. Incorporating a nitrogen doped carbon into an already conductive Cu_2O-Co_3O_4 composite resulted in the formation of a versatile catalyst. The Cu_2O-Co_3O_4/CN composite shows low overpotential compared to several other reported materials. Two metal oxides and already conducting nitrogen doped carbon improved the catalytic water splitting performance in the 1 M KOH solution. The activity diagram of the Cu_2O-Co_3O_4/CN composite is shown in Figure 8.

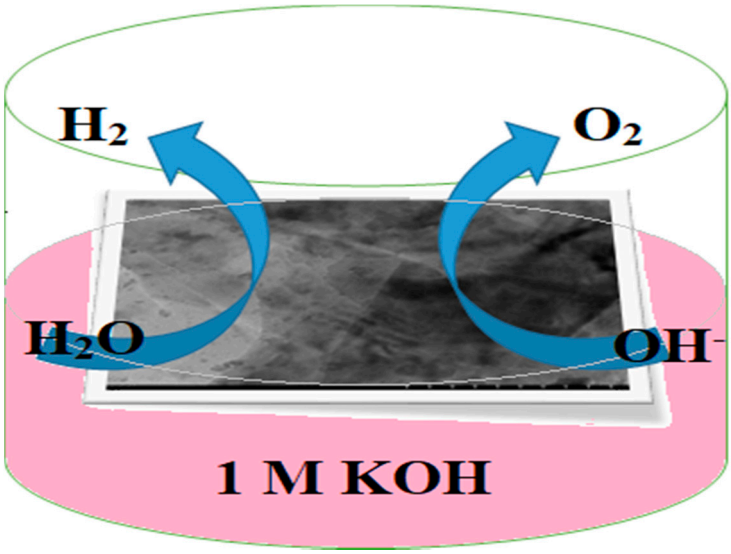

Figure 8. Activity diagram of Cu_2O-Co_3O_4/CN composite.

4. Conclusions

In combination with transition metals, such as copper and cobalt and their composites, carbon based materials are considered ideal candidates in electrocatalysis. In this research, a novel combination of nitrogen doped carbon with a cobalt oxide and copper oxide (Cu_2O-Co_3O_4/CN) composite was synthesized. The Cu_2O-Co_3O_4 composite is selected for its enhanced water splitting ability, while nitrogen doped carbon is chosen to enhance the catalyst's electrical conductivity. The synthesis was completed in two steps, at two different temperatures, and the resulting composite was used as a catalyst for electrochemical water splitting. A 1 M KOH solution was used to study the oxygen evolution reaction (OER). Different electrochemical parameters were optimized for the best conditions for water splitting. The OER efficiency of the catalysts prepared at 400 °C and 500 °C also, compared material prepared at 400 °C, showed better electrochemical performance. These results demonstrate that this combination can be used commercially for renewable energy production from water with several optimizations. Synthesis is quite easy, and the materials used for synthesis are also low cost; thus, the proposed method would be cost effective and ideal for scale up.

Author Contributions: Conceptualization, Z.A.S. and A.M.; methodology, Z.A.S. and N.M.; software, A.M. and S.Y.; writing—original draft preparation, Z.A.S. and N.M.; writing—review and editing, Z.A.S., N.M., A.M. and S.Y. All authors have read and agreed to the published version of the manuscript.

Funding: This research received no external funding.

Institutional Review Board Statement: Not applicable.

Informed Consent Statement: Not applicable.

Conflicts of Interest: The authors declare no conflict of interest.

References

1. Bekun, F.V.; Alola, A.A.; Sarkodie, S.A. Toward a sustainable environment: Nexus between CO_2 emissions, resource rent, renewable and nonrenewable energy in 16-EU countries. *Sci. Total Environ.* **2019**, *657*, 1023–1029. [CrossRef]
2. Zafar, M.W.; Shahbaz, M.; Hou, F.; Sinha, A. From nonrenewable to renewable energy and its impact on economic growth: The role of research & development expenditures in Asia-Pacific Economic Cooperation countries. *J. Clean. Prod.* **2019**, *212*, 1166–1178.
3. Hansen, K.; Mathiesen, B.V.; Skov, I.R. Full energy system transition towards 100% renewable energy in Germany in 2050. *Renew. Sustain. Energy Rev.* **2019**, *102*, 1–13. [CrossRef]
4. Gu, G.H.; Noh, J.; Kim, I.; Jung, Y. Machine learning for renewable energy materials. *J. Mater. Chem. A* **2019**, *7*, 17096–17117. [CrossRef]

5. Ivakhnenko, A.; Bakytzhan, B. Characterization of Economic and Ecological Advantages and Challenges in Development of Conventional and Unconventional Hydrocarbon, Non-Hydrocarbon and Renewable Energy Sources for Resource-Based Economy in Kazakhstan. In Proceedings of the EGU General Assembly Conference, online, 4–8 May 2020.
6. Winebrake, J.J.; Wang, M.Q.; He, D. Toxic emissions from mobile sources: A total fuel-cycle analysis for conventional and alternative fuel vehicles. *J. Air Waste Manag. Assoc.* **2001**, *51*, 1073–1086. [CrossRef]
7. Zeng, K.; Zhang, D. Recent progress in alkaline water electrolysis for hydrogen production and applications. *Prog. Energy Combust. Sci.* **2010**, *36*, 307–326. [CrossRef]
8. Tian, J.; Liu, Q.; Asiri, A.M.; Sun, X. Self-supported nanoporous cobalt phosphide nanowire arrays: An efficient 3D hydrogen-evolving cathode over the wide range of pH 0–14. *J. Am. Chem. Soc.* **2014**, *136*, 7587–7590. [CrossRef] [PubMed]
9. Hosseini, S.E.; Wahid, M.A. Hydrogen production from renewable and sustainable energy resources: Promising green energy carrier for clean development. *Renew. Sustain. Energy Rev.* **2016**, *57*, 850–866. [CrossRef]
10. Hosseini, S.E.; Wahid, M.A. Hydrogen from solar energy, a clean energy carrier from a sustainable source of energy. *Int. J. Energy Res.* **2020**, *44*, 4110–4131. [CrossRef]
11. Acar, C.; Dincer, I. Comparative assessment of hydrogen production methods from renewable and nonrenewable sources. *Int. J. Hydrogen Energy* **2014**, *39*, 1–12. [CrossRef]
12. Maggio, G.; Nicita, A.; Squadrito, G. How the hydrogen production from RES could change energy and fuel markets: A review of recent literature. *Int. J. Hydrogen Energy* **2019**, *44*, 11371–11384. [CrossRef]
13. Hisatomi, T.; Domen, K. Reaction systems for solar hydrogen production via water splitting with particulate semiconductor photocatalysts. *Nat. Catal.* **2019**, *2*, 387–399. [CrossRef]
14. Salomão, P.E.; Gomes, D.S.; Ferreira, E.J.C.; Moura, F.; Nascimento, L.L.; Patrocínio, A.O.T.; Pereira, M.C. Photoelectrochemical hydrogen production from water splitting using heterostructured nanowire arrays of Bi_2O_3/BiAl oxides as a photocathode. *Sol. Energy Mater. Sol. Cells* **2019**, *194*, 276–284. [CrossRef]
15. Fajrina, N.; Tahir, M. A critical review in strategies to improve photocatalytic water splitting towards hydrogen production. *Int. J. Hydrogen Energy* **2019**, *44*, 540–577. [CrossRef]
16. Kong, D.; Wang, H.; Cha, J.J.; Pasta, M.; Koski, K.J.; Yao, J.; Cui, Y. Synthesis of MoS_2 and $MoSe_2$ films with vertically aligned layers. *Nano Lett.* **2013**, *13*, 1341–1347. [CrossRef]
17. Faraji, M.; Yousefi, M.; Yousefzadeh, S.; Zirak, M.; Naseri, N.; Jeon, T.H.; Choi, W.; Moshfegh, A.Z. Two-dimensional materials in semiconductor photoelectrocatalytic systems for water splitting. *Energy Environ. Sci.* **2019**, *12*, 59–95. [CrossRef]
18. Wu, J.; Zhang, Y.; Zhou, J.; Wang, K.; Zheng, Y.-Z.; Tao, X. Uniformly assembling n-type metal oxide nanostructures (TiO_2 nanoparticles and SnO_2 nanowires) onto P doped g-C_3N_4 nanosheets for efficient photocatalytic water splitting. *Appl. Catalys. B Environ.* **2020**, *278*, 119301. [CrossRef]
19. Wang, J.; Cui, W.; Liu, Q.; Xing, Z.; Asiri, A.M.; Sun, X. Recent progress in cobalt-based heterogeneous catalysts for electrochemical water splitting. *Adv. Mater.* **2016**, *28*, 215–230. [CrossRef]
20. Wang, H.; Gao, C.; Li, R.; Peng, Z.; Yang, J.; Gao, J.; Yang, Y.; Li, S.; Li, B.; Liu, Z. Ruthenium-cobalt nanoalloy embedded within hollow carbon spheres as a bifunctionally robust catalyst for hydrogen generation from water splitting and ammonia borane hydrolysis. *ACS Sustain. Chem. Eng.* **2019**, *7*, 18744–18752. [CrossRef]
21. Sun, H.; Yan, Z.; Liu, F.; Xu, W.; Cheng, F.; Chen, J. Self-supported transition-metal-based electro-catalysts for hydrogen and oxygen evolution. *Adv. Mater.* **2020**, *32*, 1806326. [CrossRef]
22. Joe, J.; Yang, H.; Bae, C.; Shin, H. Metal chalcogenides on silicon photocathodes for efficient water splitting: A mini overview. *Catalysts* **2019**, *9*, 149. [CrossRef]
23. Kötz, R.; Stucki, S. Oxygen Evolution and Corrosion on Ruthenium-Iridium Alloys. *J. Electrochem. Soc.* **1985**, *132*, 103–107. [CrossRef]
24. Devarayapalli, K.C.; Lee, K.; Nam, N.D.; Vattikuti, S.V.P.; Shim, J. Microwave synthesized nano-photosensitizer of CdS QD/MoO_3–OV/g–C_3N_4 heterojunction catalyst for hydrogen evolution under full-spectrum light. *Ceram. Int.* **2020**, *46*, 28467–28480. [CrossRef]
25. Devarayapalli, K.C.; Vattikuti, S.V.P.; Sreekanth, T.V.M.; Nagajyothi, P.C.; Shim, J. Pyrolysis-Synthesized g-C_3N_4/Nb_2O_5 Nanocomposite for Enhanced Photocatalytic Activity under White LED Light Irradiation. *ChemistrySelect* **2019**, *4*, 13250–13258. [CrossRef]
26. Devarayapalli, K.; Vattikuti, S.V.P.; Sreekanth, T.V.M.; Yoo, K.S.; Nagajyothi, P.C.; Shim, J. Hydrogen production and photocatalytic activity of g-C_3N_4/Co-MOF (ZIF-67) nanocomposite under visible light irradiation. *Appl. Organomet. Chem.* **2020**, *34*, e5376. [CrossRef]
27. Vattikuti, S.P.; Devarayapalli, K.C.; Nagajyothi, P.C.; Shim, J. Microwave synthesized dry leaf-like mesoporous $MoSe_2$ nanostructure as an efficient catalyst for enhanced hydrogen evolution and supercapacitor applications. *Microchem. J.* **2020**, *153*, 104446. [CrossRef]
28. Matsumoto, Y.; Manabe, H.; Sato, E. Oxygen Evolution on $La_{1-x}Sr_x$ Fe_1-y Co y O_3 Series Oxides. *J. Electrochem. Soc.* **1980**, *127*, 2360–2364. [CrossRef]
29. Qu, Y.; Yang, M.; Chai, J.; Tang, Z.; Shao, M.; Kwok, C.T.; Yang, M.; Wang, Z.; Chua, D.; Wang, S.; et al. Facile synthesis of vanadium-doped Ni_3S_2 nanowire arrays as active electro-catalyst for hydrogen evolution reaction. *ACS Appl. Mater. Interfaces* **2017**, *9*, 5959–5967. [CrossRef]

30. Yu, Y.; Zhou, J.; Sun, Z. Novel 2D Transition-Metal Carbides: Ultrahigh Performance Electrocatalysts for Overall Water Splitting and Oxygen Reduction. *Adv. Funct. Mater.* **2020**, *30*, 2000570. [CrossRef]
31. Liu, Z.Q.; Cheng, H.; Li, N.; Ma, T.Y.; Su, Y.-Z. $ZnCo_2O_4$ quantum dots anchored on nitrogen-doped carbon nanotubes as reversible oxygen reduction/evolution electro-catalysts. *Adv. Mater.* **2016**, *28*, 3777–3784. [CrossRef] [PubMed]
32. Ding, J.; Ji, S.; Wang, H.; Gai, H.; Liu, F.; Linkov, V.; Wang, R. Mesoporous nickel-sulfide/nickel/N-doped carbon as HER and OER bifunctional electro-catalyst for water electrolysis. *Int. J. Hydrogen Energy* **2019**, *44*, 2832–2840. [CrossRef]
33. Wu, A.; Xie, Y.; Ma, H.; Tian, C.; Gu, Y.; Yan, H.; Zhang, X.; Yang, G.; Fu, H. Integrating the active OER and HER components as the heterostructures for the efficient overall water splitting. *Nano Energy* **2018**, *44*, 353–363. [CrossRef]
34. Zhang, H.; Maijenburg, A.W.; Li, X.; Schweizer, S.L.; Wehrspohn, R.B. Bifunctional heterostructured transition metal phosphides for efficient electrochemical water splitting. *Adv. Funct. Mater.* **2020**, *30*, 2003261. [CrossRef]
35. Li, Y.; Zhang, H.; Jiang, M.; Zhang, Q.; He, P.; Sun, X. 3D self-supported Fe-doped Ni_2P nanosheet arrays as bifunctional catalysts for overall water splitting. *Adv. Funct. Mater.* **2017**, *27*, 1702513. [CrossRef]
36. Wang, Z.; Xu, L.; Huang, F.; Qu, L.; Li, J.; Owusu, K.A.; Liu, Z.; Lin, Z.; Xiang, B.; Liu, X.; et al. Copper-Nickel Nitride Nanosheets as Efficient Bifunctional Catalysts for Hydrazine-Assisted Electrolytic Hydrogen Production. *Adv. Energy Mater.* **2019**, *9*, 1900390. [CrossRef]
37. Dalle, K.E.; Warnan, J.; Leung, J.J.; Reuillard, B.; Karmel, I.S.; Reisner, E. Electro- and Solar-Driven Fuel Synthesis with First Row Transition Metal Complexes. *Chem. Rev.* **2019**, *119*, 2752–2875. [CrossRef] [PubMed]
38. Roger, I.; Shipman, M.A.; Symes, M.D. Earth-abundant catalysts for electrochemical and photoelectrochemical water splitting. *Nat. Rev. Chem.* **2017**, *1*, 0003. [CrossRef]
39. Wang, J.; Choi, S.; Kim, J.; Cha, S.W.; Lim, J. Recent Advances of First d-Block Metal-Based Perovskite Oxide Electrocatalysts for Alkaline Water Splitting. *Catalysts* **2020**, *10*, 770. [CrossRef]
40. Wang, J.; Gao, Y.; Kong, H.; Kim, J.; Choi, S.; Ciucci, F.; Lim, J. Non-precious-metal catalysts for alkaline water electrolysis: Operando characterizations, theoretical calculations, and recent advances. *Chem. Soc. Rev.* **2020**, *49*, 9154–9196. [CrossRef]
41. Wang, J.; Zhao, H.; Gao, Y.; Chen, D.; Chen, C.; Saccoccio, M.; Ciucci, F. $Ba_0.5Sr_0.5Co_0.8Fe_0.2O_3-\delta$ on N-doped mesoporous carbon derived from organic waste as a bi-functional oxygen catalyst. *Int. J. Hydrogen Energy* **2016**, *41*, 10744–10754. [CrossRef]
42. Janani, G.; Yuvaraj, S.; Surendran, S.; Chae, Y.; Sim, Y.; Song, S.-J.; Park, W.; Kim, M.-J.; Sim, U. Enhanced bifunctional electrocatalytic activity of Ni-Co bimetallic chalcogenides for efficient water-splitting application. *J. Alloy. Compd.* **2020**, *846*, 156389. [CrossRef]
43. Wang, J.; Ciucci, F. Boosting Bifunctional Oxygen Electrolysis for N-Doped Carbon via Bimetal Addition. *Small* **2017**, *13*, 1604103. [CrossRef] [PubMed]
44. Wang, J.; Kim, J.; Choi, S.; Wang, H.; Lim, J. A Review of Carbon-Supported Nonprecious Metals as Energy-Related Electrocatalysts. *Small Methods* **2020**, *4*, 2000621. [CrossRef]
45. Wang, J.; Kong, H.; Zhang, J.; Hao, Y.; Shao, Z.; Ciucci, F. Carbon-based electrocatalysts for sustainable energy applications. *Progr. Mater. Sci.* **2021**, *116*, 100717. [CrossRef]
46. Surendran, S.; Sivanantham, A.; Shanmugam, S.; Sim, U.; Kalai Selvan, R. $Ni_2P_2O_7$ microsheets as efficient Bi-functional electrocatalysts for water splitting application. *Sustain. Energy Fuels* **2019**, *3*, 2435–2446. [CrossRef]
47. An, T.-Y.; Surendran, S.; Kim, H.; Choe, W.-S.; Kim, J.K.; Sim, U. A polydopamine-mediated biomimetic facile synthesis of molybdenum carbide phosphide nanodots encapsulated in carbon shell for electrochemical hydrogen evolution reaction with long-term durability. *Compos. Part B Eng.* **2019**, *175*, 107071. [CrossRef]
48. Sim, Y.; Kim, S.J.; Janani, G.; Chae, Y.; Surendran, S.; Kim, H.; Yoo, S.; Seok, D.C.; Jung, Y.H.; Jeon, C.; et al. The synergistic effect of nitrogen and fluorine co-doping in graphene quantum dot catalysts for full water splitting and supercapacitor. *Appl. Surf. Sci.* **2020**, *507*, 145157. [CrossRef]
49. Dayong, N.; Mikhaylov, A.; Bratanovsky, S.; Shaikh, Z.A.; Stepanova, D. Mathematical modeling of the technological processes of catering products production. *J. Food Process Eng.* **2020**, *43*, e13340. [CrossRef]
50. Zhang, X.; Cui, X.; Sun, Y.; Qi, K.; Jin, Z.; Wei, S.; Li, W.; Zhang, L.; Zheng, W. Nanoporous Sulfur-Doped Copper Oxide ($Cu_2O_xS_{1-x}$) for Overall Water Splitting. *ACS Appl. Mater. Interfaces* **2018**, *10*, 745–752. [CrossRef]
51. Wang, S.; He, T.; Yun, J.-H.; Hu, Y.; Ziao, M.; Du, A.; Wang, L. New Iron-Cobalt Oxide Catalysts Promoting $BiVO_4$ Films for Photoelectrochemical Water Splitting. *Adv. Funct. Mater.* **2018**, *28*, 1802685. [CrossRef]
52. Surendran, S.; Shanmugapriya, S.; Ramasamy, H.; Janani, G.; Kalpana, D.; Lee, Y.S.; Sim, U.; Selvan, R.K. Hydrothermal deposition of CoS nanostructures and its multifunctional applications in supercapattery and water electrolyzer. *Appl. Surf. Sci.* **2019**, *494*, 916–928. [CrossRef]
53. Yumashev, A.; Ślusarczyk, B.; Kondrashev, S.; Mikhaylov, A. Global Indicators of Sustainable Development: Evaluation of the Influence of the Human Development Index on Consumption and Quality of Energy. *Energies* **2020**, *13*, 2768. [CrossRef]
54. Nie, D.; Panfilova, E.; Samusenkov, V.; Mikhaylov, A. E-Learning Financing Models in Russia for Sustainable Development. *Sustainability* **2020**, *12*, 4412. [CrossRef]
55. An, J.; Mikhaylov, A.; Jung, S.-U. The Strategy of South Korea in the Global Oil Market. *Energies* **2020**, *13*, 2491. [CrossRef]
56. An, J.; Mikhaylov, A.; Kim, K. Machine Learning Approach in Heterogeneous Group of Algorithms for Transport Safety-Critical System. *Appl. Sci.* **2020**, *10*, 2670. [CrossRef]

57. Yumashev, A.; Mikhaylov, A. Development of Polymer Film Coatings with High Adhesion to Steel Alloys and High Wear Resistance. *Polym. Compos.* **2020**, *41*, 2875–2880. [CrossRef]
58. Sawant, S.Y.; Cho, M.H.; Kang, M.; Han, T.H. Carbothermal process-derived porous N-doped carbon for flexible energy storage: Influence of carbon surface area and conductivity. *Chem. Eng. J.* **2019**, *378*, 122158. [CrossRef]